Articles

Structural Insights into the A_1 ATPase from the Archaeon, *Methanosarcina mazei* Gö1†

Gerhard Grüber,*,‡ Dmitri I. Svergun,§,|| Ünal Coskun,‡ Thorsten Lemker,⊥ Michel H. J. Koch,§ Hermann Schägger,@ and Volker Müller⊥

Fachbereich Biologie/Chemie, Universität Osnabrück, D-49069 Osnabrück, Germany, Hamburg Outstation, European Molecular Biology Laboratory, EMBL c/o DESY, D-22603 Hamburg, Germany, Institute of Crystallography, Russian Academy of Sciences, 117333 Moscow, Russia, Lehrstuhl für Mikrobiologie der Ludwig-Maximilians-Universität München, D-80638 München, Germany, and Zentrum der Biologischen Chemie, Universitätsklinikum Frankfurt, D-60590 Frankfurt, Germany

Received September 18, 2000; Revised Manuscript Received December 18, 2000

ABSTRACT: The low-resolution structure and overall dimensions of the A_3B_3CDF complex of the A_1 ATPase from *Methanosarcina mazei* Gö1 in solution is analyzed by synchrotron X-ray small-angle scattering. The radius of gyration and the maximum size of the complex are 5.03 ± 0.1 and 18.0 ± 0.1 nm, respectively. The low-resolution shape of the protein determined by two independent ab initio approaches has a knob-and-stalk-like feature. Its headpiece is approximately 9.4 nm long and 9.2 nm wide. The stalk, which is known to connect the headpiece to its membrane-bound A_O part, is approximately 8.4 nm long. Limited tryptic digestion of the A_3B_3CDF complex was used to probe the topology of the smaller subunits (C−F). Trypsin was found to cleave subunit C most rapidly at three sites, Lys_{20}, Lys_{21}, and Arg_{209}, followed by subunit F. In the A_3B_3CDF complex, subunit D remained protected from proteolysis.

ATP synthases/hydrolases are present in every organism and are essential for every living cell. F-type ATPases (also called F_1F_O ATP synthases) transform energy from a transmembrane electrochemical ionic gradient (H^+ or Na^+) into the phosphoric acid anhydride bond of ATP, whereas V-type ATPases, under physiological conditions, act only as ATP-driven ion pumps. On the basis of their subunit composition and primary sequences, the archaeal enzymes are more closely related to V-type than F-type ATPases, but they function as ATP synthases, as shown in methanogens (*1*), halobacteria (*2*, *3*), and thermoacidophiles (*4*). Each enzyme is characterized by a membrane-embedded, ion-conducting complex (A_O, F_O, or V_O) and a hydrophilic portion (A_1, F_1, or V_1) in which ATP synthesis and/or hydrolysis takes place. Whereas nucleotide-binding subunits A and B of the A and V ATPase are homologous to the F ATPase β and α subunits, respectively, it is difficult to identify regions of similarity of the smaller A_1, F_1, and V_1 subunits (*5*, *6*). Three-dimensional models of the F_1 and V_1 ATPase show the alternating α/β and A/B subunits arranged hexagonally, interdigitating for most of their length (*7*−*10*). The hexameric moiety is connected via a stalk to the ion-translocating portion. Structural comparison of the F_1 and V_1 stalks indicates different shapes and lengths of these stalk regions (*11*−*14*).

Despite the fact that A ATPases reveal chimeric properties of F and V ATPases, the mechanism of ATP synthesis by A ATPases remains a mystery. This problem is largely due to the instability of the isolated complexes and the resulting lack of detailed information about the structure of this enzyme. In an ongoing project dealing with the molecular mechanism of ATP synthesis in methanogenic archaea, the A_1 encoding genes from *Methanosarcina mazei* Gö1 have been overexpressed in *Escherichia coli* DK8, and the overexpressed A_1 complex has been characterized.[1] This complex is made up of the five different subunits (A−D and F) with apparent molecular masses of 64, 51, 41, 24, and 11 kDa, respectively, as estimated from the amino acid sequences (*15*). In the work presented here, two independent methods have been used to retrieve the low-resolution structure of the hydrated A_1 ATPase of *M. mazei* ab initio from X-ray small-angle scattering. The resulting overall shape allows one to determine the similarities and differences regarding the closely related F_1 and V_1 ATPases. Together with protease digestion studies of the A_1 complex, the low-

† This research was supported by grants from the Deutsche Forschungsgemeinschaft to V.M. (Mu801/10-1), H.S. (SFB 472), and G.G. (GR 1475/6-1), the International Association for the Promotion of Cooperation with Scientists from the Independent States of the Former Soviet Union (INTAS) to D.I.S. and M.H.J.K. (Grant 96-1115), and EU Biotechnology Program Grant BIO4-CT97-2143 to D.I.S.

* To whom correspondence should be addressed: Fachbereich Biologie/Chemie, Universität Osnabrück, D-49069 Osnabrück, Germany. Phone: +49/(0)541 969 3504. Fax: +49/(0)541 969 3503. E-mail: ggrueber@biologie.uni-osnabrueck.de.

‡ Universität Osnabrück.

§ European Molecular Biology Laboratory.

|| Russian Academy of Sciences.

⊥ Lehrstuhl für Mikrobiologie der Ludwig-Maximilians-Universität München.

@ Universitätsklinikum Frankfurt.

[1] T. Lemker and V. Müller, manuscript in preparation.

10.1021/bi002195t CCC: $20.00
Published on Web 01/26/2001

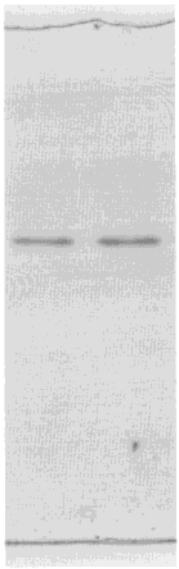

FIGURE 1: Analysis of the purified A_3B_3CDF complex before and after exposure to X-rays. The A_1 complex (6 μg) was analyzed before (lane 1) and after (lane 2) exposure to X-rays by nondenaturing PAGE.

resolution structure has been used to explore the topology of the individual subunits. The rates of cleavage of individual subunits of A_1 are discussed in terms of their function.

MATERIALS AND METHODS

Materials. All chemicals were at least of analytical grade and were obtained from BIOMOL (Hamburg, Germany), Merck (Darmstadt, Germany), Sigma (Deisenhofen, Germany), or Serva (Heidelberg, Germany).

Purification of the A_1 ATPase. The A_1 ATPase from *M. mazei* Gö1 was obtained from *E. coli* strain DK8 expressing the A_1 ATPase genes A−F on a multicopy vector pTL2. The enzyme was isolated by gel permeation chromatography and subsequently ion exchange chromatography, as will be described elsewhere.[1] For solution X-ray scattering experiments (see below), the enzyme was subsequently applied onto a Sephacryl S-300 HR column (10/30, Pharmacia) equilibrated in 50 mM Tris[2]-HCl (pH 7.0) and 150 mM NaCl and subjected to gel permeation chromatography (FPLC) to isolate a homogeneous A_1 complex. The purity and homogeneity of the protein sample were analyzed by native polyacrylamide gel electrophoresis (*16*) and SDS−PAGE (*17*). Protein bands on SDS gels were stained with Coomassie Brilliant Blue G250. Protein concentrations were determined according to the method of Lowry (*18*). ATPase activity was measured at 37 °C in an assay mixture containing 100 mM MES (pH 5.2), 40 mM $NaHSO_3$, 10 mM $MgSO_4$, and 10% (v/v) glycerol. The reaction was started by the addition of ATP at a final concentration of 4 mM. The ATPase activity was determined by the extent of release of inorganic phosphate which was measured at a wavelength of 355 nm as described by Heinonen and Lahti (*19*).

X-ray Scattering Experiments and Data Analysis. The synchrotron radiation X-ray scattering data were collected

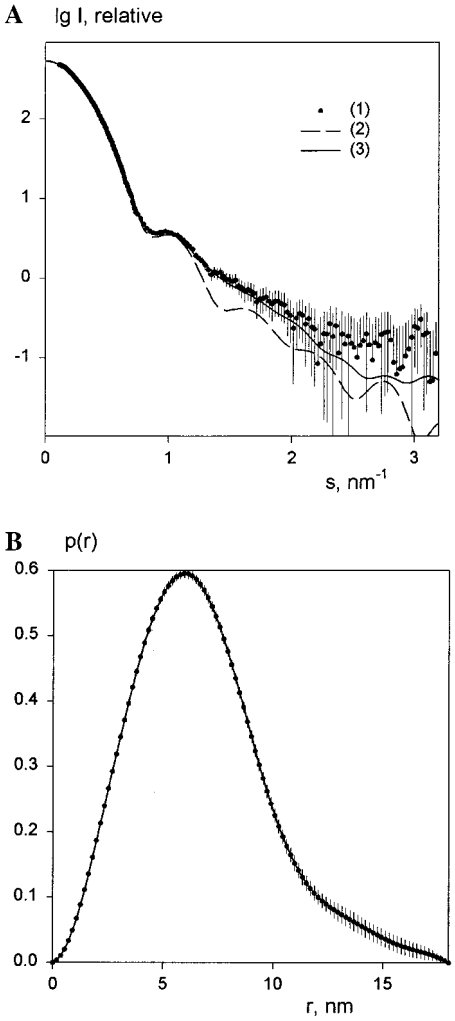

FIGURE 2: Experimental and calculated scattering data of the A_1 complex. (A) X-ray scattering curves for the A_1 ATPase: composite experimental curve (1), scattering from the model envelope (2), and scattering from the dummy atom model (3). (B) Distance distribution function of the A_1 ATPase evaluated by the program GNOM.

following standard procedures on the X33 camera (*20*−*22*) of the EMBL on the storage ring DORIS III of the Deutsches Elektronen Synchrotron (DESY) using multiwire proportional chambers with delay line readout (*23*). Solutions with protein concentrations of 4.5 and 10 mg/mL were measured. At sample−detector distances of 3.9 and 1.4 m and a wavelength λ of 0.15 nm, the ranges of momentum transfer (s) from 0.14 to 2.1 nm^{-1} and from 0.08 to 5.0 nm^{-1} were covered ($s = 4\pi \sin \theta/\lambda$, where 2θ is the scattering angle). The data were normalized to the intensity of the incident beam and corrected for the detector response; the scattering of the buffer was subtracted, and the difference curves were scaled for concentration using the program SAPOKO (D. I. Svergun and M. H. J. Koch, unpublished).

The maximum dimension D_{max} of the A_1 ATPase was estimated from the experimental curves, using the orthogonal expansion program ORTOGNOM (*24*). The distance distribution functions $p(r)$ and the radii of gyration R_g were computed by the indirect Fourier transform program GNOM (*25*, *26*). The molecular masses of the solutes were estimated by comparison with forward scattering data from a reference solution of bovine serum albumin.

[2] Abbreviations: PAGE, polyacrylamide gel electrophoresis; SDS, sodium dodecyl sulfate; Tris, tris(hydroxymethyl)aminomethane.

The low-resolution particle shape was restored from the experimental data using two ab initio procedures. In the method of Svergun et al. (*27*, *28*), the particle shape is represented by an angular envelope function $r = F(\omega)$, where r and ω are spherical coordinates. The envelope is parametrized as

$$F(\omega) = \sum_{l=0}^{L} \sum_{m=-l}^{l} F_{lm} Y_{lm}(\omega) \quad (1)$$

where $Y_{lm}(\omega)$ are spherical harmonics and the multipole coefficients f_{lm} are complex numbers. The scattering intensity $I(s)$ from the envelope is evaluated by the method of Svergun (*24*) as

$$I(s) = 2\pi^2 \sum_{l=0}^{\infty} \sum_{m=-l}^{l} |A_{lm}(s)|^2 \quad (2)$$

where the partial amplitudes $A_{lm}(s)$ are calculated from the coefficients f_{lm} (*25*). The program SASHA (*24*, *27*) determines these coefficients by minimizing the discrepancy defined as

$$R^2 = \sum_{k=1}^{N} \{W(s_k)[I(s_k) - I_{exp}(s_k)]\}^2 / \sum_{k=1}^{N} [W(s_k) I_{exp}(s_k)]^2 \quad (3)$$

where N is the number of the experimental points, the weighting function $W(s_k)$ $\{=s_k^2/[\sigma(s_k)/I_{exp}(s_k)]$, $I_{exp}(s_k)$, and $\sigma(s_k)\}$ is the experimental intensity with its standard deviation in the kth point. Series 1 contains $M = (L + 1)^2 - 6$ free parameters and provides a spatial resolution δr of approximately $\sqrt{5\pi}R_g/[\sqrt{3}(L + 1)]$.

In the second ab initio procedure using the DAMMIN program (*28*), a sphere of diameter D_{max} is filled with densely packed small spheres (dummy atoms) with radii $r_0 \ll D_{max}$. The structure of the dummy atom model (DAM) is defined by a configuration vector **X**, assigning an index to each atom corresponding to a solvent (0) or solute particle (1). The scattering intensity from the DAM is computed using eq 2 with the partial amplitudes (*28*)

$$A_{lm}(s) = i^l \upsilon_a \sqrt{2/\pi} \sum_j j_l(sr_j) Y_{lm}(\omega_j) \quad (4)$$

where the sum runs over the dummy atoms where $X_j = 1$ (particle atoms), r_j, and ω_j are their polar coordinates, $\upsilon_a = (4\pi r_0^3/3)/0.74$ is the displaced volume per dummy atom, and $j_l(x)$ denotes the spherical Bessel function. In keeping with the low resolution of the solution scattering data, the method searches for a configuration X minimizing $f(X) = \chi^2 + \alpha P(X)$. Here, χ denotes the discrepancy between the calculated and experimental curves

$$\chi = \sqrt{\frac{1}{N-1} \sum_{j=1}^{N} \left[\frac{I(s_j,X) - I_{exp}(s_j)}{\sigma(s_j)}\right]^2} \quad (5)$$

where N is the number of the experimental points and $I_{exp}(s_k)$ and $\sigma(s_k)$ are the experimental intensity and its standard deviation, respectively. The "looseness" penalty term $P(X)$ ensures that configuration X yields a compact and interconnected structure and $\alpha > 0$ is a penalty weight selected to have significant penalty contribution at the end of the minimization. The latter is performed starting from a random configuration and using the simulated annealing algorithm [SA (*28*)]; details of the procedure are described elsewhere (*28*, *29*).

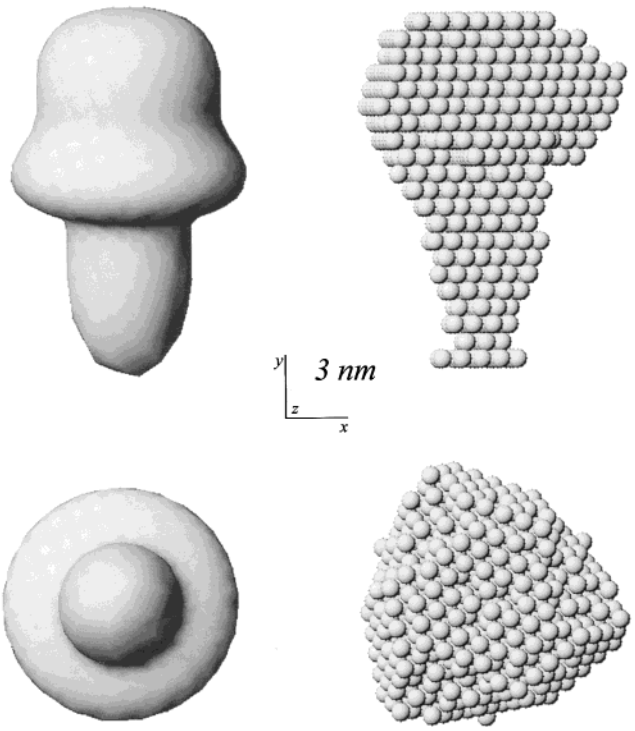

FIGURE 3: Low-resolution models of the A_3B_3CDF complex of the A_1 ATPase. (Left) Envelope model and (right) a DAM obtained by simulated annealing. The bottom rows are rotated counterclockwise by 90° around the *Y*- and *X*-axes. The models were displayed on an IBM-PC/NT workstation using the program MASSHA.[3]

Prior to the shape analysis, a constant is subtracted from the experimental data to ensure that the intensity decays as s^{-4} following Porod's (*30*) law for homogeneous particles. The value of this constant is determined automatically by DAMMIN from the outer part of the curve by linear regression of $s^4I(s)$ versus s^4. This procedure yields an approximation of the "shape-scattering" curve (i.e., scattering due to the excluded volume of the particle filled by a constant density).

SASHA and DAMMIN also allow one to incorporate additional information about particle symmetry and anisometry. The models were derived from the experimental data assuming a 3-fold symmetry for the entire molecule, which is justified given that the major part of the A_1 ATPase possesses a quasi-3-fold symmetry (*10*, *15*). The symmetry restrictions result in a significant reduction in the number of free parameters in the models. The asymmetry of the enzyme cannot be meaningfully analyzed at low resolution.

Trypsin Digestion Studies. A_1 ATPase was incubated at a concentration of 5.9 mg/mL with trypsin in a ratio of 900:1 (w/w) in 20 mM Tris-HCl (pH 7.5) and 150 mM NaCl at 30 °C. Trypsin cleavage was stopped by addition of the protease inhibitor Pefabloc SC (8 mM). Afterward, the protein samples were applied to a gel for electrophoresis [17.5% total acrylamide (T) and 0.4% cross-linked acrylamide (C)]. For identification of the trypsin fragments, the protein samples were blotted on a polyvinylidene difluoride

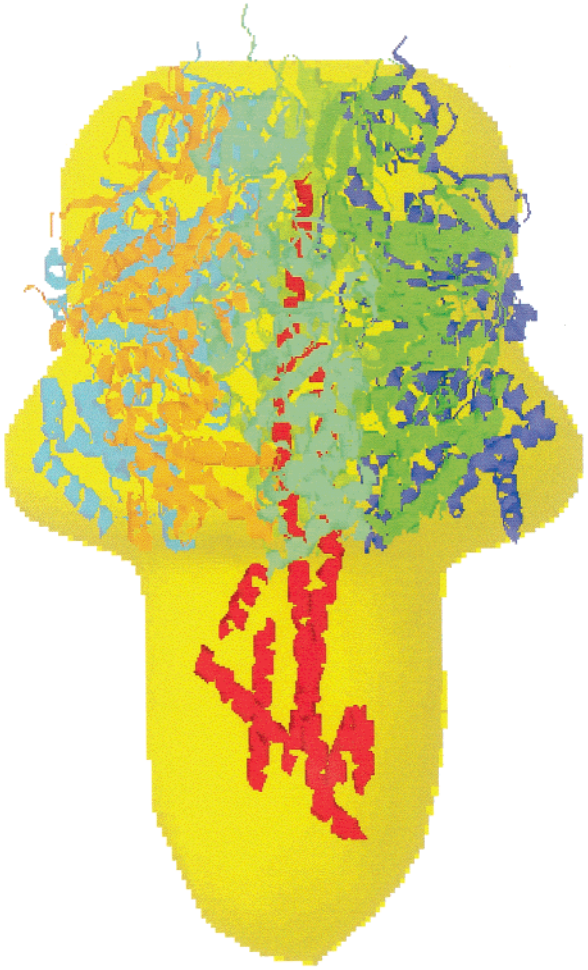

FIGURE 4: RASMOL drawing of the polypeptide backbone of the $\alpha_3\beta_3\gamma$ subunits of the *E. coli* F_1 ATPase using the crystallographic coordinates of Brookhaven Protein Data Bank (*43*) entry 1D8S (*34*). The structure is superimposed on an envelope of the A_3B_3CDF complex of the A_1 ATPase from *M. mazei*.

membrane (pore size of 0.45 μm; Bio-Rad) (*31*). Filter pieces with the respective fragments were used directly for N-terminal sequence analysis using a protein sequencer (model 473A, Applied Biosystems). The identity of proteolytic fragments was also resolved by use of antisera against subunits A−C and F as described in ref *15*. The generation of the antisera will be described elsewhere.[1]

RESULTS AND DISCUSSION

Overall Dimensions and Shape of the A_3B_3CDF Complex. The A_1 ATPase from *M. mazei* Gö1, containing the five subunits (A−D and F), was isolated to high purity and homogeneity (Figure 1). The ATP hydrolysis rate as isolated was 8 ± 0.5 μmol of ATP hydrolyzed per milligram of protein per minute. The composite X-ray solution scattering of the A_1 complex is shown in Figure 2. The complex has a maximum dimension of 18.0 ± 0.1 nm and a radius of gyration of 5.03 ± 0.1 nm (Figure 2B). Qualitative analysis of the distance distribution function suggests that the enzyme consists of a globular core yielding a principal maximum in the $p(r)$ at $0 < r > 12$ nm with a protuberance giving rise to a shoulder between 12 and 18 nm (Figure 2B). The Porod volume of the hydrated particle is 710 ± 20 nm^3, in good agreement with the molecular mass estimation of the complex

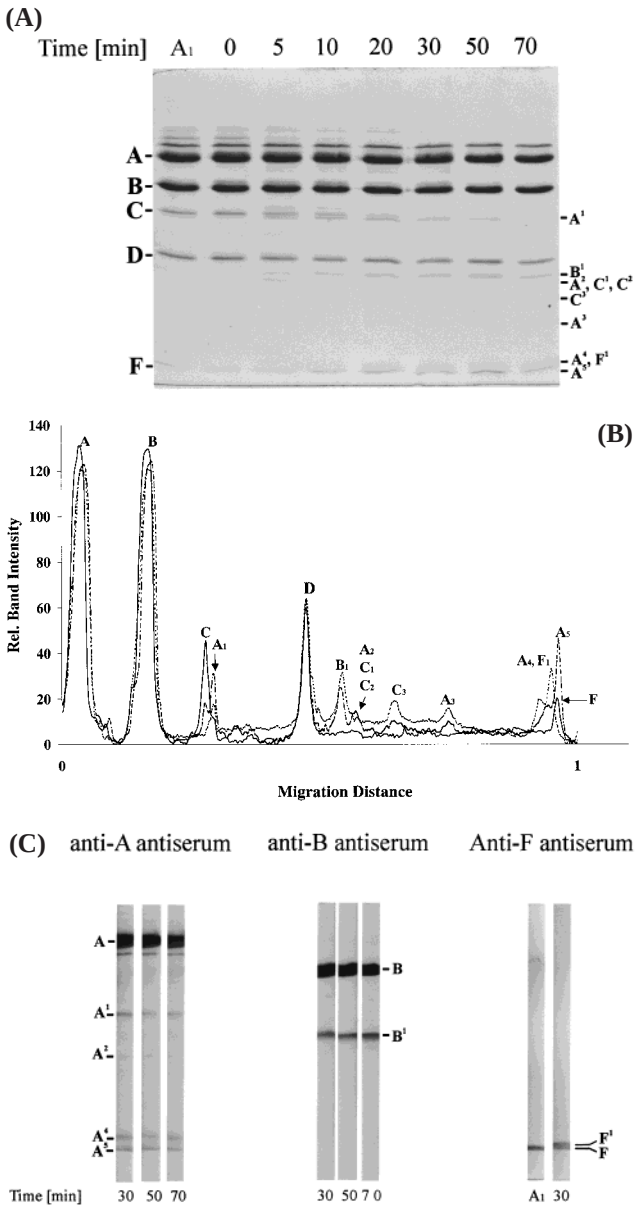

FIGURE 5: Time course of trypsin cleavage of A_1 ATPase from *M. mazei*. (A) A_1 ATPase (6 μg) was incubated with trypsin (900:1, w/w) for the indicated time before the reaction was stopped by addition of the protease inhibitor Pefabloc SC (8 mM). Samples were electrophoresed on a 17.5% total acrylamide and 0.4% cross-linked acrylamide gel. (B) Density scanning profile of A_1 ATPase before (—) and after 20 (-·-) and 70 min (···) of proteolysis. The image analysis was performed using the program Quantity One (Bio-Rad). (C) Immunoblot of the same samples in the time course of 30−70 min with antibodies against the A and B subunits and immunoblots of the untreated and trypsinized (30 min) A_1 complex with an antiserum directed against the F subunit.

calculated from the amino acid sequence (*15*), native gel electrophoresis, and gel filtration.[1]

The shape scattering curve in the range of the momentum transfer up to an s_{max} of 3.0 nm^{-1} was used to restore the low-resolution particle shape with two ab initio procedures, assuming that the particle had a 3-fold symmetry axis. The outer part of the curve contained a significant contribution from the scattering of internal structure and was discarded

[3] P. V. Konarev, M. V. Petoukhov, and D. I. Svergun, manuscript in preparation.

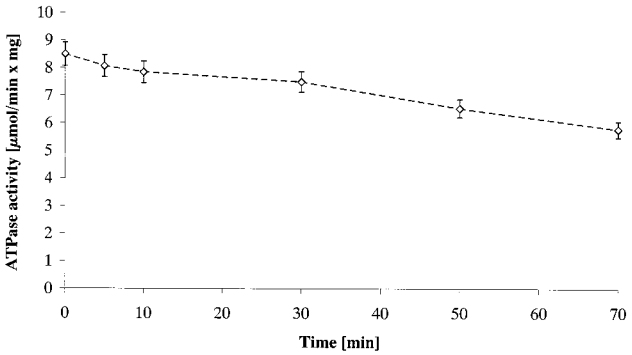

FIGURE 6: Effect of proteolysis on the enzyme activity of the A_1 ATPase.

in the shape analysis. Shape determination using the envelope function (eq 1) is unique when the number of Shannon channels (*32*, *33*) in the data $N_s = s_{max}D_{max}/\pi$ exceeds 1.5 times the number (M) of parameters describing the envelope. The shape scattering curve of A_1 ATPase contains 17.2 (N_s) channels and allows one to use harmonics up to $L = 6$ ($M = 17$), providing a spatial resolution δr of 3.0 nm. The restored envelope in Figure 3, left column, yields the fit to the data in Figure 2A with a residual R_I of 7×10^{-3}, a radius of gyration R_g of 5.10 nm, and an excluded volume V_p of 737 nm^3.[3]

In the second ab initio procedure, a sphere with a diameter D_{max} of 18.0 nm was filled by 4213 densely packed dummy atoms with radii r_0 of 0.5 nm. The restored structure at a default penalty weight α of 0.01 (Figure 3, right column) contains 1020 dummy atoms, yields an R_g of 5.11 nm and a V_p of 722 nm^3, and fits to the experimental data with a χ of 0.66 (curve 3 in Figure 2A).

Both shape determination methods independently yield a similar low-resolution structure with a headpiece which is approximately 9.4 nm long and 9.2 nm wide. Superposition of the low-resolution structure of the A_1 complex with the atomic model of the $\alpha_3\beta_3\gamma$ complex of the closely related F_1 ATPase from *E. coli* (*34*) reveals a striking similarity, especially with respect to the disposition of the nucleotide binding F_1 subunits α and β, with homologous A_1 subunits B and A, respectively (Figure 4). This structural similarity lends support to the view that A and F ATPases share a common catalytic mechanism for ATP synthesis. The overall structure of the hydrated particle is asymmetric due to the stalk which is approximately 8.4 nm long and 6.0 nm in diameter. These structural features are also found in negatively stained images of the *M. mazei* A_1A_O which show a headpiece approximately 10 nm in diameter and a stalk that accounts for linking the catalytic site events with proton pumping in the A_O portion (*15*, *35*). A stalk with the dimensions shown in Figure 4 could accommodate subunits C−F with a total molecular mass of about 80 kDa, assuming a C_1:D_1:F_1 stoichiometry. The shape and length of the stalk domain of the A_1 ATPase strongly resemble those of the closely related V_1 ATPase from *Manduca sexta*, which is approximately 11 nm in length, as determined from solution X-ray scattering [Figure 7 (*14*)]. In contrast, the low-resolution structure and atomic model of the *E. coli* F_1 ATPase (*14*, *34*) and the most recently determined crystallographic model of the complete bovine F_1 ATPase ($\alpha_3\beta_3\gamma\delta\epsilon$) (*36*) reveal that the stalk of the F_1 ATPase is significantly shorter, approximately 4.0−4.5 nm in length and 5.0−5.3 nm wide [Figure 7 (*7*, *14*, *34*, *36*)]. This pattern is consistent with the proposed close evolutionary linkage of A_1 and V_1 ATPases, which are thought to have evolved from common ancestral genes (*5*, *37*).

Trypsin Treatment of the A_1 ATPase. Protease digestion studies of the A_3B_3CDF complex were undertaken to

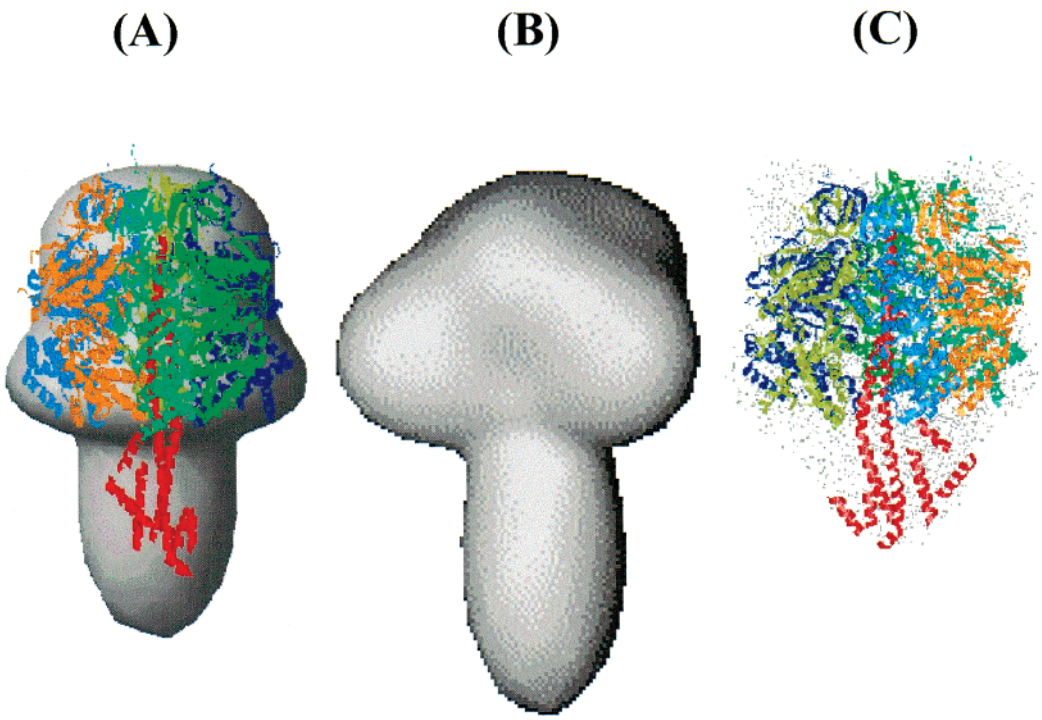

FIGURE 7: Comparison of the low-resolution envelopes of the A_1 (A), V_1 (B) (*14*), and F_1 ATPases (C) (*14*, *44*). The atomic model of the *E. coli* $\alpha_3\beta_3\gamma$ subcomplex (*34*) is positioned inside the low-resolution envelope of the A_1 complex from *M. mazei* and the low-resolution model of the hydrated *E. coli* F_1 ATPase ($\alpha_3\beta_3\gamma\delta\epsilon$; shown in gray sticks).

Table 1: Amino-Terminal Sequences of A−C Subunit Fragments after Trypsin Cleavage

subunit fragment	N-terminal sequence
A^1	$_{300}$EAXXYTGXTLAE$_{311}$
A^2	$_{365}$AXXAETLCGE$_{374}$
A^3	$_{454}$AMDMLQTESELQEIV$_{468}$
B^1	$_{271}$GYPGYMYT$_{278}$
C^1	$_{21}$KGXXNYAYA$_{29}$
C^2	$_{22}$GXXNYAYAVT$_{31}$
C^3	$_{210}$XKDRKLF$_{216}$

examine the topology of the smaller subunits (C−F), as well as the functional importance of individual subunits of this enzyme. The time course of proteolysis was probed by SDS−PAGE, in which the trypsin-treated samples were compared with a control sample of untreated A_1 ATPase (Figure 5A,B). The first stalk subunit which is cut is subunit C followed by subunit F, which becomes cleaved into fragment F^1 (up to 30 min), resulting in a slightly slower migration in the gel as shown by immunoblotting (Figure 5C); it implies that both subunits are exposed in the complex. Cleavage of subunit C leads to fragments C^1 and C^2 and with prolonged incubation with trypsin to the disappearance of C, C^1, and C^2 and the formation of C^3 (up to 30 min). N-Terminal sequence analysis suggests that the cleavage of products C^1−C^3 occurred after residues Lys_{20}, Lys_{21}, and Arg_{209}, respectively (Table 1). The accessibility of trypsin to subunit C is consistent with the assembly of the evolutionary linked V_1 ATPase in which subunit C, which is homologue to the C subunit of A_1 as shown by the immunotechnique (not shown), is at the periphery of the stalk (*10*). In the intact A_3B_3CDF complex of the A_1 ATPase, subunit D was well-protected from the effect of trypsin. A scan of the lanes of the untreated and trypsinized A_1 complex indicates a similar quantitation of the staining intensity of subunit D before and after proteolysis (Figure 5B). The shielding to trypsin of subunit D is an important finding since this subunit has been proposed as a structural and functional homologue of the γ subunit of F ATPases (*15*), which is partly intercalated into the cavity of the $\alpha_3\beta_3$ hexamer [Figure 4 (*7*−*9*, *34*)] and protected by stalk subunit ϵ (*38*, *39*).

The nucleotide-binding subunits A and B were cleaved in relatively small amounts, leading to fragments B^1, A^1, and A^2, as analyzed by immunoblotting using antibodies against subunits A and B (Figure 5C). With longer incubation times (up to 30 min), fragments A^3−A^5 are formed. Protein sequencing of polypeptides B^1 and A^1−A^3 indicates that the protease cleavage occurred after residues Arg_{270}, Arg_{299}, Arg_{364}, and Arg_{453}, respectively.

The time course of trypsinolysis was also examined by ATPase activity of the A_1 complex (Figure 6). After trypsin treatment for 10 min, the ATPase activity was slightly inhibited by 10% more than before proteolysis. There was also significant removal of the C subunit and partial clipping of subunits A and B, based on SDS−PAGE. Prolonged proteolysis (30 min) results in ∼30% inhibition of ATPase activity and a higher yield of fragments B^1, A^3−A^5, C^3, and F^1. However, the remaining complex containing subunits A, B, and D still retains a high ATPase activity. By comparison, prolonged digestion of the related *E. coli* F_1 ATPase with trypsin resulted in an active complex retaining the core subunits α, β, and γ (*40*, *41*). This pattern is consistent with the comparison of the kinetic properties of $\alpha_3\beta_3$ and $\alpha_3\beta_3\gamma$ complexes from the thermophilic *PS3* F_1 ATPase, indicating that the γ subunit is necessary for catalytic promotion and active site cooperativity (*42*).

In summary, the quaternary structures obtained using two ab initio shape restoration procedures show independently that the A_3B_3CDF complex of the A_1 ATPase is organized as two well-defined domains, with a knoblike domain approximately 9.2 nm in diameter and 9.4 nm in height, presumably containing the alternating three copies each of subunits A and B and a stalk approximately 8.4 nm in length. Trypsin digestion studies left an active core complex containing subunits A, B, and D, implying a central arrangement of subunit D in the A_3B_3 core. The observation that subunits C and F are susceptible to trypsin places them at the periphery of the stalk. In the near future, electron micrographs of the A_3B_3CDF complex labeled with an antibody to subunit D may reveal the spatial arrangement in the complex and thus provide the basis for exploring its function.

REFERENCES

1. Becher, B., and Müller, V. (1994) *J. Bacteriol. 176*, 2543−2550.
2. Mukohata, Y., Isoyama, M., and Fuke, A. (1986) *J. Biochem. 99*, 1−8.
3. Mukohata, Y., and Yoshida, M. (1987) *J. Biochem. 101*, 311−318.
4. Dirmeier, R., Hauska, G., and Stetter, K. O. (2000) *FEBS Lett. 467*, 101−104.
5. Müller, V., Ruppert, C., and Lemker, T. (1999) *J. Bioenerg. Biomembr. 31*, 15−27.
6. Bowman, B. J., and Bowman, E. J. (1997) in *The Mycota III. Biochemistry and Molecular* Biology (Brambl, R., and Marzluf, G., Eds.) pp 57−83.
7. Gogol, E. P., Lücken, U., Bork, T., and Capaldi, R. A. (1989) *Biochemistry 28*, 4709−4716.
8. Abrahams, J. P., Leslie, A. G. W., Lutter, R., and Walker, J. E. (1994) *Nature 370*, 621−628.
9. Bianchet, M. A., Hullihen, J., Pedersen, P. L., and Amzel, M. L. (1998) *Proc. Natl. Acad. Sci. U.S.A. 95*, 11065−11070.
10. Grüber, G., Radermacher, M., Ruiz, T., Godovac-Zimmermann, J., Canas, C., Kleine-Kohlbrecher, D., Huss, M., Harvey, W. R., and Wieczorek, H. (2000) *Biochemistry 39*, 8609−8616.
11. Dschida, W., and Bowman, B. J. (1992) *J. Biol. Chem. 267*, 18783−18789.
12. Boekema, E. J., Ubbink-Kok, T., Lolkema, J. S., Brisson, A., and Konings, W. N. (1998) *Photosynth. Res. 57*, 267−273.
13. Wilkens, S., Vasilyeva, E., and Forgac, M. (1999) *J. Biol. Chem. 274*, 31804−31810.
14. Svergun, D. I., Konrad, S., Huss, M., Koch, M. H. J., Wieczorek, H., Altendorf, K., Volkov, V. V., and Grüber, G. (1998) *Biochemistry 37*, 17659−17663.
15. Wilms, R., Freiberg, C., Wegerle, E., Meier, I., Mayer, F., and Müller, V. (1996) *J. Biol. Chem. 271*, 18843−18852.
16. Schägger, H., and von Jagow, G. (1991) *Anal. Biochem. 199*, 223−231.
17. Laemmli, U. K. (1970) *Nature 227*, 680−685.
18. Lowry, O. H., Rosebrough, N. J., Farr, A. L., and Randall, R. J. (1951) *J. Biol. Chem. 193*, 265−275.
19. Heinonen, J. K., and Lahti, R. J. (1981) *Anal. Biochem. 113*, 313−317.
20. Koch, M. H. J., and Bordas, J. (1983) *Nucl. Instrum. Methods 208*, 461−469.
21. Boulin, C., Kempf, R., Koch, M. H. J., and McLaughlin, S. M. (1986) *Nucl. Instrum. Methods A249*, 399−407.
22. Boulin, C. J., Kempf, R., Gabriel, A., and Koch, M. H. J. (1988) *Nucl. Instrum. Methods A269*, 312−320.

23. Gabriel, A., and Dauvergne, F. (1982) *Nucl. Instrum. Methods 201*, 223−224.
24. Svergun, D. I. (1993) *J. Appl. Crystallogr. 26*, 258−267.
25. Svergun, D. I., Semenyuk, A. V., and Feigin, L. A. (1988) *Acta Crystallogr. A44*, 244−250.
26. Svergun, D. I. (1992) *J. Appl. Crystallogr. 25*, 495−503.
27. Svergun, D. I., Volkov, V. V., Kozin, M. B., and Stuhrmann, H. B. (1996) *Acta Crystallogr. A52*, 419−426.
28. Svergun, D. I. (1999) *Biophys. J. 76*, 2879−2886.
29. Svergun, D. I., Malfois, M., Koch, M. H. J., Wigneshweraraj, S. R., and Buck, M. (2000) *J. Biol. Chem. 275*, 4210−4214.
30. Porod, G. (1982) General Theory, in *Small-angle X-ray scattering* (Glatter, O., and Kratky, O., Eds.) pp 17−51, Academic Press, London.
31. Matsudaira, P. (1987) *J. Biol. Chem. 262*, 10035−10038.
32. Shannon, C. E., and Weaver, W. (1949) *The mathematical theory of communication*, University of Illinois Press, Urbana, IL.
33. Moore, P. B. (1980) *J. Appl. Crystallogr. 13*, 168−175.
34. Hausrath, A. C., Grüber, G., Matthews, B. W., and Capaldi, R. A. (1999) *Proc. Natl. Acad. Sci. U.S.A. 96*, 13697−13702.
35. Mayer, F., Jussofie, A., Salzmann, M., Lübben, M., Rohde, M., and Gottschalk, G. (1987) *J. Bacteriol. 169*, 2307−2309.
36. Gibbons, C., Montgomery, M. G., Leslie, A. G. W., and Walker, J. E. (2000) *Nat. Struct. Biol. 7*, 1055−1061.
37. Nelson, N. (1992) *Biochim. Biophys. Acta 1100*, 109−124.
38. Soteropoulos, P., Suss, K.-H., and McCarthy, R. E. (1992) *J. Biol. Chem. 267*, 10348−10354.
39. Tang, C., Wilkens, S., and Capaldi, R. A. (1994) *J. Biol. Chem. 269*, 4467−4472.
40. Smith, J. B., and Sternweis, P. C. (1982) *Arch. Biochem. Biophys. 217*, 376−387.
41. Gavilanes-Ruiz, M., Tommasino, M., and Capaldi, R. A. (1988) *Biochemistry 27*, 603−609.
42. Kaibara, C., Matsui, T., Hisabori, T., and Yoshida, M. (1996) *J. Biol. Chem. 271*, 2433−2438.
43. Bernstein, F. C., Koetzle, T. F., Williams, G. J. B., Meyer, E. G., Jr., Brice, M. D., Rodgers, J. R., Kennard, O., Shimanouchi, T., and Tasumi, M. (1977) *J. Mol. Biol. 112*, 535−542.
44. Grüber, G. (2000) *J. Bioenerg. Biomembr. 32*, 341−346.

BI002195T